Ortho-substituted aryldiazonium design for defect configuration-controlled photoluminescent functionalization of chiral single-walled carbon nanotubes

Boda Yu[1], Sadahito Naka[1], Haruka Aoki[1], Koichiro Kato[1,2], Tsuyohiko Fujigaya[1,2,3*], Tomohiro Shiraki[1,3*]

[1] Department of Applied Chemistry, Graduate School of Engineering, Kyushu University, 744 Motooka, Nishi-ku, Fukuoka 819-0395, Japan

[2] Center for Molecular Systems (CMS), Kyushu University, 744 Motooka, Nishi-ku, Fukuoka 819-0395, Japan.

[3] International Institute for Carbon-Neutral Energy Research (WPI-I2CNER), Kyushu University, 744 Motooka, Nishi-ku, Fukuoka, 819-0395, Japan.

[*] Email: shiraki.tomohiro.992@m.kyushu-u.ac.jp; fujigaya.tsuyohiko.948@m.kyushu-u.ac.jp

Abstract

Defect functionalization using chemical modification of single-walled carbon nanotubes (SWCNTs) is promising, especially for near-infrared photoluminescence (NIR PL) over 1000 nm in advanced telecom and bio/medical applications. The covalent attachment of modifier molecules is utilized to create sp^3 carbon defects in the sp^2 carbon lattice for bright, red-shifted PL generation. The positional difference in proximal sp^3 carbons, known as the defect binding configuration, can dominate NIR PL properties; however, the defect arrangement chemistry remains unelucidated. We developed aryldiazonium modifiers with π-conjugated *ortho*-substituents (phenyl and acetylene groups) to introduce molecular interactions with nanotube sidewalls into the chemical reaction process for defect formation. Single defect emissions of ~1230–1270 nm selectively appeared in the functionalized chiral SWCNTs, showing a different binding configuration from those observed for typical aryl- or alkyl-functionalized chiral tubes emitting approximately 1150-nm PL. Moreover, the acetylene-based substituent design allows PL brightening and subsequent molecular modification using click chemistry.

Introduction

The surface chemistry of nanomaterials is an important aspect for the functionalization and development of nanotechnology applications. Chemical modification of the surfaces of carbon materials is a widely used technique for functionalization.[1,2] As a new feature of chemical functionalization, the enhancement of near-infrared (NIR) photoluminescence (PL) properties has recently been observed for single-walled carbon nanotubes (SWCNTs).[3, 4, 5, 6, 7] SWCNT structures are defined by the chiral index (n,m) determined by the direction of the rolling vectors in the graphitic lattice to form the cylindrical structures and semiconducting properties appear in some chiral "(n,m), n≠m" and zigzag "(n,0)" architectures although armchair "(n,n)" SWCNTs are metallic. For semiconducting SWCNTs, the electronic band structures are formed based on the van Hove singularity that arises from their well-defined one-dimensional nanoarchitectures; the corresponding inter-band transitions are observed. [8, 9, 10] The lowest energy transition, denoted as the E_{11} transition, relates to PL generated by a radiative recombination process of the exciton, which is a quasi-particle state of an excited electron and the corresponding hole. A significant drawback of SWCNT PL is their very low photoluminescence quantum yield (PLQY), which is caused by the quenching processes of mobile excitons in SWCNTs such as tube edge collision[11] and low-lying exciton states[12]. The capturing the mobile excitons and their efficient conversion to PL has been achieved by limited chemical functionalization, namely local chemical functionalization. This functionalization allows local sp^3 carbon defects to be doped into the crystalline sp^2 carbon network structures of SWCNTs through chemical bond formation with modifier molecules such as aryldiazonium salts and alkyl halides. As a result, the locally functionalized SWCNTs (lf-SWCNTs) newly show defect PL with longer wavelengths and higher PLQYs compared to that of the E_{11} PL from pristine tubes.[3, 4, 5, 6, 7] These materials are also known as organic color centers (OCCs) or defect-doped SWCNTs. The wavelength changes in the defect PL for lf-SWCNTs can be observed based on structures and functions of the functionalized molecules including the substituent electronic property differences in the functionalized aryl groups,[13, 14] supramolecular assembling using molecular recognition[15, 16] and dynamic covalent bonding systems,[17] and divalent functionalization.[18, 19] Based on the theoretical and experimental results, our divalent functionalization studies suggested that the relative positions of two proximal sp^3 carbons could be a crucial factor for defect PL wavelength variation.[18, 19]

Typically, chiral (6,5)-rich SWCNTs, which are commercially available or sorted by separation techniques such as aqueous two phase methods,[20, 21] are used. The defect PL from lf-SWCNTs with (6,5) chirality has been mainly observed in the 1100–1200 nm region for E_{11}* PL and to a limited extent in the >1200 nm region for E_{11}*$^-$ PL[22, 23], also denoted as $E_{11}{}^2$* [18, 19, 24] and E_{11}** PL[25, 26], respectively. Diazonium chemistry is one of the most frequently used techniques for local chemical functionalization. This reaction mechanism is based on that phenyl radical or phenyl cation generated from aryldiazonium salts attack the nanotube walls and the resultant radical or cation on the tubes

could induce the addition reaction of another aryldiazonium reactant or hydrogen/hydroxy group from solvents or surfactants to form an additional sp^3 carbon in its proximity.[27, 28] Gifford et al. systematically simulated proximal defect models for the doped sites of lf-SWCNTs. They reported a correlation between the position of the two proximal sp^3 carbons, described as defect binding configuration (Supplementary Fig. 1), and observed defect PL regions for E_{11}* PL and E_{11}*$^-$ PL.[6, 29, 30] They determined the location of the sp^3 carbons to be either adjacent to the site of the first sp^3 carbon ("Ortho") or three carbon atoms away ("Para") together with angles from the nanotube axis in density functional theory (DFT) and time-dependent DFT (TD-DFT) calculations. Based on this, the defect binding configurations (OrthoL90 and OrthoL30 shown in Supplementary Fig. 1) were found to relate to E_{11}* PL (~1150 nm) and E_{11}*$^-$ PL (~1250 nm), respectively, for lf-SWCNTs with (6,5) chirality. In addition, they reported that the tube symmetry strongly contributed to the resulting defect binding configuration; the zigzag SWCNTs mainly demonstrated E_{11}*$^-$ PL, whereas the chiral SWCNTs like (6,5) tubes typically demonstrated E_{11}* PL.[31, 32] As described above, it was shown that the defect binding configuration for E_{11}* PL or E_{11}*$^-$ PL generation could be dominated by the tube structures rather than the difference in modifier molecules in the diazonium reactions. Therefore, the surface chemistry of SWCNTs for selective defect formation, regardless of the tube structure, remains a challenge and significant issue, especially for E_{11}*$^-$ PL generation in the abundant chiral SWCNTs. It is imperative to understand the chemical reactions occurring on the π-conjugated surfaces of the nanotubes, and to control the selective formation of specific defect binding configurations for the modulation of defect PL from lf-SWCNTs. In particular, the generation of E_{11}*$^-$ PL with longer wavelengths and deep optical trap depths would be beneficial for the exciton engineered materials such as a single photon emitter used in quantum technologies.[3]

In our previous study, the local chemical functionalization using aryldiazonium salts with -NO_2, -Br, or -CH_3 groups in the *orthro* position produced lf-SWCNTs that simultaneously showed defect PL at ~1150 and ~1300 nm.[33] This indicates that *ortho*-substituents of the aryldiazonium salts may affect a reaction process for the defect binding configuration formation in the lf-SWCNT synthesis. However, the aryldiazonium modifiers cannot produce selective E_{11}*$^-$ PL, and further investigation is necessary to clarify the *orthro* substituent effects in lf-SWCNT synthesis and to achieve defect binding configuration control. In this study, E_{11}*$^-$ PL for chiral SWCNTs were selectively created using aryldiazonium salts with π-conjugated *ortho*-substituents (*o*X-Dz). The modifier design was based on the molecular interactions of the *ortho*-substituents that affected the π electron systems of the tube surfaces in the reaction process to form a defect binding configuration. Using *o*X-Dz for the local chemical functionalization selectively produced E_{11}*$^-$ PL from the lf-(6,5)SWCNTs and other chiral lf-SWCNTs. In addition, acetylene-based *ortho*-substituents allow PL brightening and post-molecular modification of the doped sites by click chemistry for the lf-SWCNTs-*o*X.

Results and discussion

Optical properties of the lf-SWCNTs

The *o*X-Dz (X = phenyl acetylene (PA), phenyl (P), and acetylene (A)) was synthesized by diazotization of each aniline precursor. The SWCNTs (CoMoCAT, (6,5) chirality rich) were solubilized in micellar solutions of sodium dodecyl sulfate (SDS) in D_2O to create a homogeneous reaction system for local chemical functionalization. These SWCNT solutions were mixed with *o*X-Dz at room temperature for 7 days to synthesize *ortho*-aryl functionalized lf-SWCNTs (lf-SWCNTs-*o*X). To investigate the effects of the substituent positions of the aryl isomers, *para*- and *meta*-substituted aryldiazonium salts tethering a PA group were similarly synthesized and reacted with SWCNTs to synthesize *para*- and *meta*-aryl functionalized lf-SWCNTs (denoted as lf-SWCNTs-*p*PA and lf-SWCNTs-*m*PA, respectively).

Fig. 1a shows the PL spectra of lf-SWCNTs-*p*PA, -*m*PA, -*o*PA, and pristine SWCNTs. The excitation wavelength was 570 nm, which corresponded to the second lowest van Hove transition (E_{22} transition) of the (6,5) chirality tubes.[34] The observed PL at 980 nm was attributed to a signal from the E_{11} transition of pristine SWCNTs and of pristine sites in lf-SWCNTs-*p*PA, -*m*PA, and -*o*PA.[34] Compared to the E_{11} PL, the red-shifted PL was observed for lf-SWCNTs-*p*PA, -*m*PA, and -*o*PA at 1143, 1143, and 1260 nm, respectively. The PL signals of lf-SWCNTs-*p*PA and -*m*PA were observed in wavelength regions similar to those in the typical E_{11}* PL in reported *para*- and *meta*-substituted aryl functionalized lf-SWCNTs.[33] In contrast, lf-SWCNTs-*o*PA showed a significant red-shifted PL with high selectivity. In diazonium chemistry for (6,5) SWCNTs functionalization, a typical E_{11}* PL appeared at ~1150 [11,13]. Such PL at~1250 nm were detected limitedly in divalent [18, 19] or high degree chemical modifications.[18, 23, 29] Therefore, lf-SWCNTs-*o*PA was further characterized in terms of local chemical functionalization. Fig. 1b shows the normalized PL spectra of lf-SWCNTs-*o*PA when the concentrations of *o*PA-Dz were changed for the synthesis (for the original PL spectra, see Supplementary Fig. 2a). By increasing the *o*PA-Dz concentration to 0.64 μM, the PL intensity at 1260 nm increased due to the formation of defect doped sites. In contrast, for the increase to 1.28 μM *o*PA-Dz, the intensity decreased because of being too defective by over functionalization. In the UV/vis/NIR absorption spectra of lf-SWCNTs-*o*PA shown in Fig. 1c, the E_{11} transition absorbance at 980 nm partially decreased in response to the increase in *o*PA-Dz concentrations. The Raman spectra of lf-SWCNTs-*o*PA (Fig. 1d) showed peaks at approximately 1300 and 1580 cm^{-1} that were assigned to the D band originating from the introduction of sp^3 defects into the graphitic sp^2 lattice and the G band originating from the graphitic carbon lattice vibration, respectively.[35] The intensity ratio values of the D to G band (D/G) increased with the increase in *o*PA-Dz concentration (Supplementary Fig. 2b), thus revealing sp^3 carbon defect introduction through the reaction between the SWCNT walls and *o*PA-Dz. These spectroscopic results were consistent with those observed in typical lf-SWCNTs.[4, 5, 7] Therefore, local chemical functionalization using *o*PA-Dz to dope sp^3 carbon defects successfully

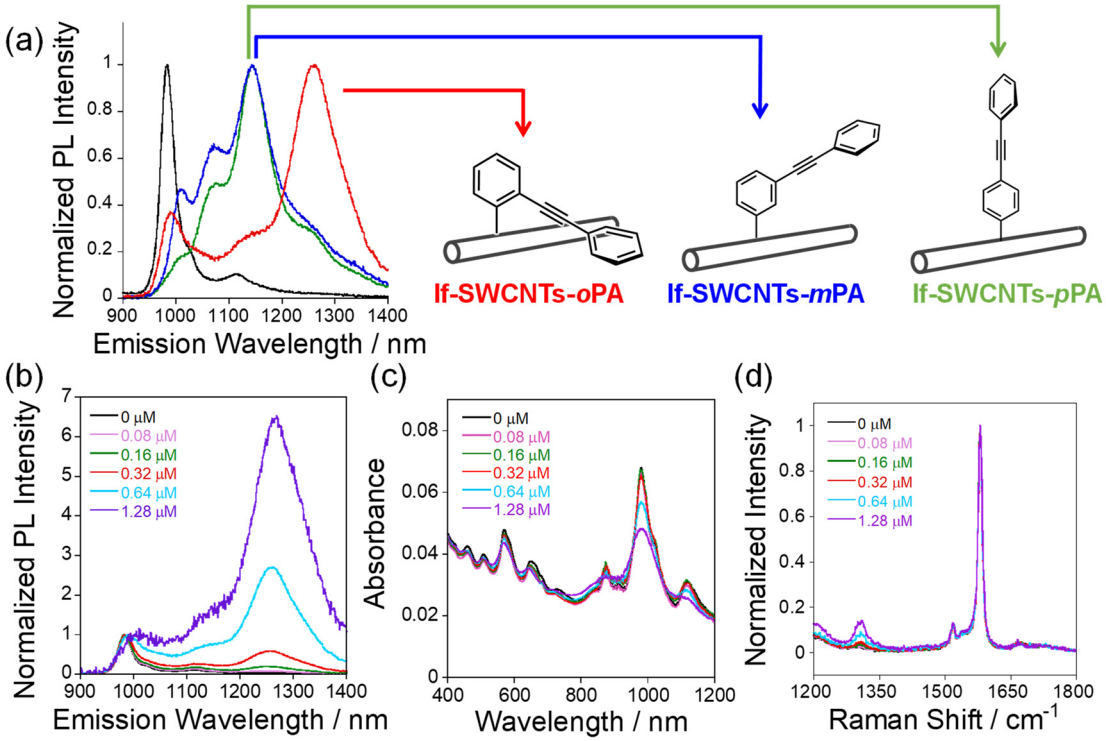

Fig. 1. Optical characterization of lf-SWCNTs. **a.** PL spectra of pristine SWCNTs (black), lf-SWCNTs-*o*PA (red), -*m*PA (blue), and -*p*PA (green) at the reactant diazonium concentration of 0.64 μM. **b.** PL spectra of lf-SWCNTs-*o*PA at different concentrations of *o*PA-Dz. **c.** Absorption spectra of lf-SWCNTs-*o*PA. **d.** Raman spectra of lf-SWCNTs-*o*PA.

occurred to produce the defect emission at 1260 nm (E_{11}*$^{-}$ PL) in lf-SWCNTs-*o*PA.

The other *ortho*-substituted aryldiazonium salts with different conjugated substituents of an acetylene group (*o*A-Dz), a phenyl group (*o*P-Dz) and a vinyl group (*o*V-Dz) were investigated. These structures were chosen to modulate the π conjugation of the *ortho* substituents for nanotube interactions. That is, the *o*P and *o*A substituents were designed to investigate the acetylene linker and phenyl end groups, respectively, by eliminating them from the *o*PA substituent structure. The *o*V substituent was designed for a bond structural change from the triple to double bond. The PL spectra of lf-SWCNTs synthesized using *o*P-Dz, *o*A-Dz, or *o*V-Dz (lf-SWCNTs-*o*A, lf-SWCNTs-*o*P and lf-SWCNTs- *o*V, respectively) are shown in Fig. 2a–c. For all samples, the defect PL (> 1200 nm) was observed in wavelength regions longer than E_{11} PL (~980 nm) by means of this functionalization. In addition, the UV/vis/NIR absorption and Raman spectral measurements (Supplementary Fig.3 a–c) showed that local chemical functionalization of SWCNTs using *o*P-Dz, *o*A-Dz, or *o*V-Dz has successfully occurred, similarly to lf-SWCNTs-*o*PA. From the viewpoint of the PL properties, lf-SWCNTs-*o*P showed a defect emission selectively at 1263 nm, and its PL intensities were comparable

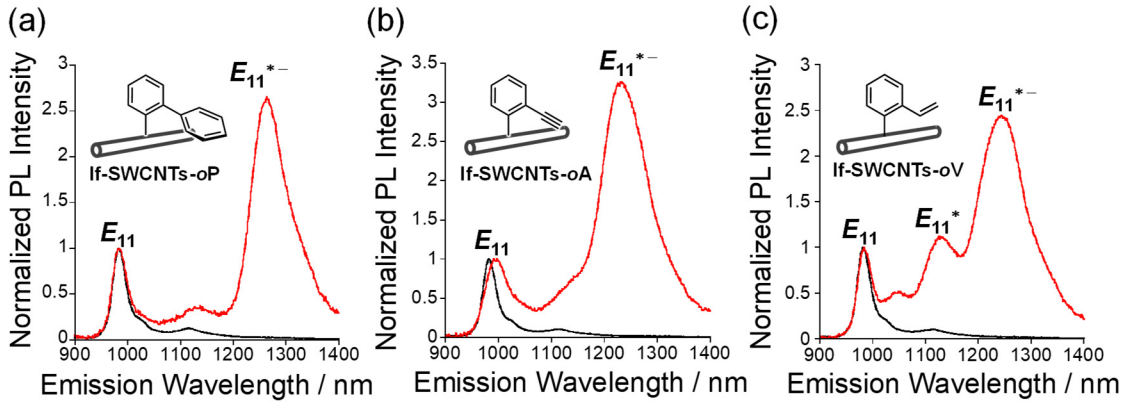

Fig. 2. PL spectra of pristine SWCNTs (black) lf-SWCNTs synthesized using *o*X-Dz (red); **a.** lf-SWCNTs-*o*P **b.** lf-SWCNTs-*o*A **c.** lf-SWCNTs-*o*V.

to those of lf-SWCNTs-*o*PA. For lf-SWCNTs-*o*A, a defect emission was also selectively observed at ~1230 nm. In addition, the intensities increased by approximately 20% compared to the highest intensity of lf-SWCNTs-*o*PA, which had similar defect degrees based on the D/G values obtained via Raman spectroscopy. This result indicates that bulkiness of the end group contributes to emission efficiency of the defect PL. This characteristic is specifically discussed in the following section for PL enhancement observation. In contrast, lf-SWCNTs-*o*V showed two defect PL peaks simultaneously at ~1128 and ~1243 nm, revealing low wavelength selectivity for defect PL generation. In the molecular modeling investigation shown in Supplementary Fig. 4, the *o*P and *o*PA groups parallelly aligned on the tube surfaces in lf-SWCNTs-*o*P and -*o*PA. In contrast, the *o*V deviated from its parallel position to the tube surface because of steric hinderance from the hydrogen atoms in the double-bond structure. Therefore, interactions based on π electrons of the *ortho* substituents play an important role in the selective generation of E_{11}^{*-} PL. Specifically, molecular interactions such as π–π interactions between the substituents and sp^2 hybridized SWCNT walls are expected to contribute extensively to the resulting PL properties. This inference is discussed further in the theoretical simulation studies described in Supplementary Information.

PL intensity enhancement based on substituent structures

As described above, the end group structures of the *ortho*-substituents contributed to the defect PL intensities. This finding was the motivation for further structural designs of *o*X-Dzs, and we found that this factor could be applied to brighten E_{11}^{*-} PL. In this study, a phenyl diacetylene group was introduced (*o*PdA-Dz) that was designed to enlarge the distance between the end phenyl group of the *ortho*-substituent and tube wall, to avoid steric hindrance. The PL spectra of lf-SWCNTs synthesized using *o*PdA-Dz (lf-SWCNTs-*o*PdA) is shown in Fig. 3 (PL spectra without peak normalization are

shown in Supplementary Fig. 5). The E_{11}^{*-} PL intensity at 1262 nm dramatically increased compared to that of lf-SWCNTs-*o*PA (Supplementary Fig. 2) and lf-SWCNTs-*o*A with the same degrees of defect introduction based on the D/G values (Supplementary Fig. 6). Absolute PLQY measurements (Supplementary Table 1) revealed that the PLQY value of lf-SWCNTs-*o*PdA was 1.54 times higher than that of lf-SWCNTs-*o*PA. In contrast, when the trimethylsilyl group with sp^3 hybridized bulky architecture was attached to the end of the *ortho*-acetylene and diacetylene groups (*o*SA and *o*SdA, respectively), the resulting lf-SWCNTs (lf-SWCNTs-*o*SA and -*o*SdA) showed significantly decreased intensities for the defect PL at 1256 and 1238 nm, respectively, as shown in Supplementary Fig. 7a and b, compared to lf-SWCNTs-*o*PA and -*o*A, and lf-SWCNTs-*o*PdA.

To investigate the steric effects, we examined the closest distance (d_c) of the end groups from the tube walls in the molecular modeling for each doped site (Supplementary Fig. 8). The d_c values were increased from 0.296 nm for *o*A to 0.367 and 0.390 nm for *o*PA and *o*PdA, respectively, based on the increase in linker lengths. The introduction of silyl end groups remarkably decreased the d_c values to 0.290 and 0.295 nm for lf-SWCNTs-*o*SA and -*o*SdA, respectively. Therefore, steric hindrance could decrease emission efficiency of the defect PL by causing strain on the tube structures that affects geometry and electronic structures. This strain-induced PL quenching has been reported in pristine SWCNTs and other low-dimensional nanomaterials.[36, 37] Therefore, the mechanism for the observed PL brightening is based on avoiding nonradiative relaxation pathways by the π-linker elongation design through the *ortho*-substituents of *o*X-Dzs. The electron-withdrawing nature of *para*-substituents of aryldiazonium salts used for lf-SWCNT synthesis is reported[13] but mostly unknown molecular factor for enhancing defect PL intensities of lf-SWCNTs. Our findings revealed that another factor is the chemical modification-induced strain in the tube structures that could remarkably affect the defect PL intensities, and that the molecular effects can be tunable based on the molecular design of the modifiers. Moreover, additional PL brightening was achieved by changing the surfactants used

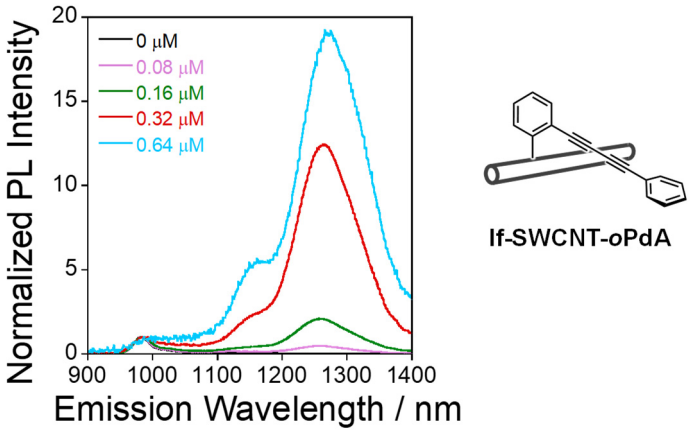

Fig. 3. Normalized PL spectra for lf-SWCNTs-*o*PdA synthesized using different concentrations of *o*PdA-Dz.

for solubilizing lf-SWCNTs in the aqueous media. As shown in Supplementary Fig. 9, the defect PL intensity was increased 2.53 times by changing SDS to sodium dodecylbenzenesulfonate (SDBS) for lf-SWCNTs-*o*PdA. A 1.98 times-enhancement in the intensity was observed for sodium deoxycholate (DOC). Compared to lf-SWCNTs-*o*P in SDS solutions, a PL intensity greater than 6.07 times was achieved by the molecular design and surfactant exchange to SDBS for lf-SWCNTs-*o*PdA.

Surfactant environment effects for E_{11}^{*-} generation in lf-SWCNTs-*o*X

The experimental results in the previous section indicated that direct interactions and spatial molecular arrangements of the *ortho*-substituents in the aryl group contributed to the resultant defect binding configuration of the sp^3 carbons for E_{11}^{*-} PL generation (~1250 nm) in lf-SWCNTs. The reported simulation studies indicated that the defect PL at ~1150 nm (E_{11}^{*} PL) and ~1250 nm (E_{11}^{*-} PL) for the lf-SWCNTs with (6,5) chirality correlated with the defect binding configurations of OrthoL90 and OrthoL30, respectively (For a schematic image of the binding configuration, see Supplementary Fig. 1).[6, 30, 38] The E_{11}^{*} PL typically appears in ~1150 nm wavelength regions in the diazonium chemistry for lf-SWCNTs synthesis using (6,5) SWCNTs, even when various modifiers with different chemical structures are used.[5] Therefore, the interactions between the π conjugated *ortho*-substituents were considered to effectively change the defect binding configuration from typical OrthoL90 to rare OrthoL30 in diazonium chemistry using (6,5) SWCNTs. To further investigate the *ortho*-substituent interactions for selective E_{11}^{*-} PL generation in lf-SWCNTs-*o*X, surfactants coated onto the tube surfaces were altered in the local chemical functionalization process, in which the effects of surrounding environments creating reaction fields were expected to appear in the defect binding configuration.

In fact, when SDBS, which is known to tightly adsorb on the tube surface,[39] was used instead of SDS, the E_{11}^{*-} PL (1262 nm) selectivity was decreased, and E_{11}^{*} PL was observed at 1151 nm (Supplementary Fig. 10a). This suggests that OrthoL90 defect binding configuration was also produced because of fewer interactions between the tube wall and *ortho*-substituents in this reaction environment. Moreover, in the SDBS system, the concentration of used diazonium salts needed to be one order higher than those required in the SDS condition. This indicates that a higher concentration diazonium salt is needed to react with the SWCNT surfaces to compete with the tightly adsorbed SDBS. A similar selectivity decrease in the E_{11}^{*-} PL generation and high concentrations of used diazonium salts were observed in other surfactants of cationic cetyltrimethylammonium chloride (CTAC) and neutral polyethylene glycol tert-octylphenyl ether (Triton-X), as shown in Supplementary Fig. 10b and c. Consequently, SDS provides most ideal environment for E_{11}^{*-} PL generation among the used surfactants in the *o*X-Dz functionalization because SDS provides a relatively favorable interface atmosphere for the interactions between the *ortho*-substituents and tube walls.

E_{11}^{*-} PL generation for other chiral SWCNTs

In previous diazonium chemistry studies using typical *para*-substituted aryldiazonium salts for lf-SWCNT synthesis, it was reported that the preferential binding configuration strongly depended on tube structures.[30,31] In contrast, we found that the *o*X-Dzs were applicable to various SWCNTs for E_{11}^{*-} generation, regardless of their chirality and modality. (Note: Modality is a SWCNT structure classification using n and m numbers in the chiral indices based on the remainder when the difference between *n* and *m* is divided by three, showing mod (n-m,3) =1 and 2.[40, 41]) Herein, (7,5)SWCNTs in the used commercial (6,5)-rich SWCNT sample were investigated, in which the modality of (6,5) and (7,5)SWCNTs were classified as mod(n-m,3) =1 and = 2, respectively.[42] Furthermore, other chiral (9,4) and (8,6)SWCNTs in a commercial (7,6)-rich SWCNT sample were investigated.

For example, lf-(7,5)SWCNTs-*o*PdA showed a defect PL at 1257 nm that was significantly red-shifted than E_{11}^{*} PL at 1143 nm of lf-SWCNTs synthesized using *p*PA-Dz (Supplementary Fig. 11). In the three dimensional (3D) PL mapping image of the sample (Supplementary Fig. 12), the 645 nm excitation that corresponded to the E_{22} transition of (7,5)SWCNTs generated PL at 1257 nm. Therefore, the 1257-nm PL for lf-(7,5)SWCNTs-*o*PdA was recognized as E_{11}^{*-} PL from the doped sites created by the reaction with *o*PdA-Dz (Fig. 4a and b). The observed E_{11}^{*-} PL selectivity, regardless of the tube modality in the *o*PdA-Dz functionalization, had a completely new trend compared to the previous report that showed the generation of E_{11}^{*} PL and E_{11}^{*-} PL for mod (n-m,3) =1 and 2 tubes, respectively.[38] The E_{11}^{*-} PL was observed in all the lf-SWCNT samples used in this experiment, including 1350 nm for lf-(7,6)SWCNTs-*o*PdA, 1289 nm for lf-(9,4)SWCNTs-*o*PdA, and 1374 nm for lf-(8,6) SWCNTs-*o*PdA (Supplementary Fig. 13). These E_{11}^{*-} PLs appeared in longer wavelength

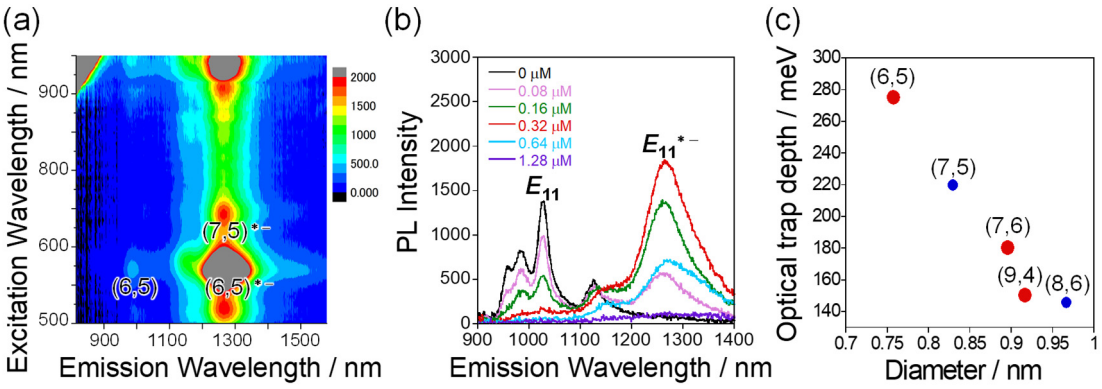

Fig. 4. PL spectra of lf-SWCNTs-*o*PdA under different condition. a. PL mapping image of lf-SWCNTs-*o*PdA synthesized using (6,5) rich SWCNTs that contain (7,5) tubes. **b.** PL spectra of lf-(7,5)SWCNTs-*o*PdA excited at 645 nm. The concentrations of *o*PdA-Dz were changed from 0.08 to 1.28 μM. **c.** Optical trap depths of E_{11}^{*-} PL as a function of the SWCNT diameters.

regions than the reported E_{11}* PLs from lf-SWCNTs with identical chiralities.[13] In addition, the optical trap depths of E_{11}*$^{-}$ PL for each chirality tube were decreased linearly when the diameter of the nanotube[34] increased, which concurred with previous studies (Fig. 4c).[43] Therefore, our *ortho*-substituent design allows selective generation of E_{11}*$^{-}$ PL for SWCNTs with different modalities and chiralities, and offers novel chemical tools for PL wavelength modulation in lf-SWCNT synthesis.

Subsequent molecular functionalization of doped sites in lf-SWCNTs-*o*A using click chemistry

The acetylene-based molecular design of *o*A-Dz that produced bright E_{11}*$^{-}$ PL in the lf-SWCNTs could provide a chemical reaction for further functionalization of the doped sites through click chemistry such as Huisgen 1,3-dipolar cycloaddition.[44] In particular, these diverse molecular attachment systems have a great potential for applications in various fields using the functionalized doped sites of lf-SWCNTs.[17, 45] In this study, a copper-catalyzed azide-alkyne cycloaddition (CuAAC) reaction was performed using lf-SWCNTs-*o*A. Briefly, 4-azido-2,3,5,6-tetrafluorobenzoic acid (ATFB), Cu(II)SO_4, tris(3-hydroxypropyltriazolylmethyl)amine (THPTA), and sodium ascorbate were added to a lf-SWCNTs-*o*A solution, and heated for 2 h at 80°C. For the control experiment, a small molecule of *p*-ethynylbenzoic acid was used to confirm the corresponding triazole product formation under the reaction condition. The resultant lf-SWCNTs (F-lf-SWCNTs) were collected by vacuum filtration, carefully washed to remove unreacted reagents and surfactants, and dried in vacuum. The resultant F-lf-SWCNTs sheets were analyzed by X-ray photoelectron spectroscopy (XPS).

Table 1 shows the estimated atomic concentrations of C, N, and F before and after CuACC functionalization. For F-lf-SWCNTs. A decrease in the C value and increase in the N and F values in the atomic concentrations were observed after the reaction treatment. Since the ATFB reagent has N and F atoms, the result suggests that the tetrafluorobenzoic acid group is introduced by the CuAAC reaction. Note, the small amount of N and F signal detected in the pristine SWCNTs could be attributed to small amounts of physical adsorption of the reagent molecules on the tube wall.[43] Fig. 5 shows the XPS spectra for F 1s and N 1s orbitals of the pristine SWCNTs after the CuAAC reaction treatment and F-lf-SWCNTs. In the F 1s spectra, a small peak was detected at ~689 eV in the pristine SWCNTs, which was assigned to the C–F bonds of physically adsorbed ATFB reagents.[46] For F-lf-SWCNTs, a large peak appeared at ~688 eV. In the peak deconvoluted spectrum (Supplementary Fig. 14a), the new signal at 688 eV was clearly verified as a different peak at 689 eV observed even for the pristine tubes, indicating covalent attachment of the tetrafluorobenzoic acid group.[47] In the N 1s spectra, F-lf-SWCNTs showed a distinct peak at 402 eV. The peak deconvolution (Supplementary Fig. 14b) revealed that two peaks located at ~400 and ~402 eV were detected, which related to the N=N and C-N bonds in the triazole group.[48] In the pristine SWCNT sample, very small peaks were observed at ~399 and ~403 eV relating to the N/N and N^{+} signals, respectively, of the physically adsorbed ATFB

reagents.[49] Therefore, the successful cycloaddition reaction on lf-SWCNTs-*o*A was confirmed, thus covalent post-modification using the click reaction was achieved on the doped sites of lf-SWCNTs based on the *ortho*-alkyne motif of the modifiers used in this study. Regarding PL properties, the CuAAC reaction treatment resulted in a slight spectral shift of the E_{11}^{*-} PL (~9 nm). Click chemistry, including CuAAC reactions, allows for the modification of various molecules such as organic dyes, biomolecules; therefore, versatile functionalization of the lf-SWCNTs could be developed based on this concept.

Table 1. Atomic concentrations of each atom for C, N, and F, estimated by XPS analysis of the pristine SWCNTs after the CuACC reaction treatment and F-lf-SWCNTs.

	C	N	F
pristine SWCNTs	99.0 ± 0.20	0.63 ± 0.14	0.41 ± 0.07
F-lf-SWCNTs	97.2 ± 0.24	1.97 ± 0.15	0.85 ± 0.15

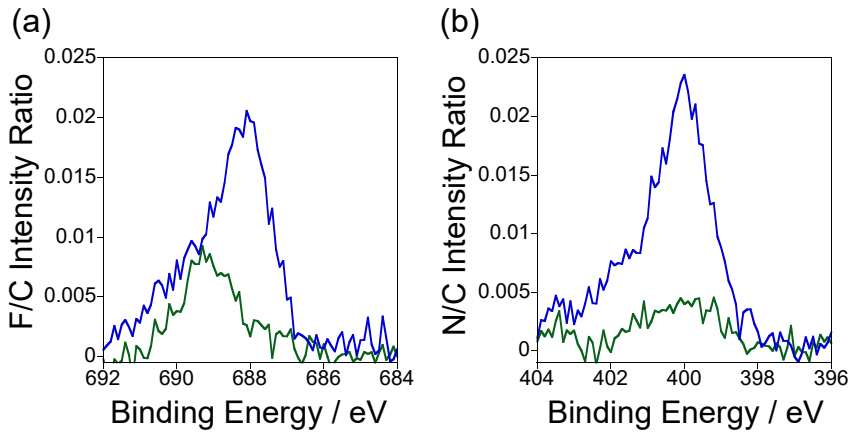

Fig. 5. XPS spectra. a. F 1s and **b.** N 1s orbitals of the pristine SWCNTs after the CuACC reaction treatment (green) and F-lf-SWCNTs (blue).

Conclusion

We designed *ortho*-substituted aryldiazonium salts with π-conjugated substituents for local chemical functionalization of SWCNTs and initiated the selective generation of E_{11}^{*-} PL as a defect PL from the doped sites of the resulting lf-SWCNTs-*o*X synthesized by diazonium chemistry.

PLQY enhancement with the unique E_{11}^{*-} PL selectivity was observed by varying the substituent structure, wherein the elongation of the acetylene linkers, to avoid steric interference of the end phenyl groups to the tube surfaces, increased emission efficiency, as seen in lf-SWCNTs-*o*PdA. In total, 6.07 times brightening was achieved by this molecular design with the assistance of the surfactant exchange from SDS to SDBS compared to the initial lf-SWCNTs-*o*P.

Moreover, the E_{11}^{*-} PL can be selectively created for various SWCNTs regardless of their chiralities and modalities. This is a significantly different trend from previously reported aryldiazonium reactions; that is, in the typical aryl modification, E_{11}^{*} PL was observed as defect PL in chiral lf-SWCNT such as (6,5) tubes because the E_{11}^{*} PL or E_{11}^{*-} PL selectivity was dominated by tube structures such as chiral/zigzag architectures and modalities. Thus, this *ortho*-substituted modifier motif offers a universal design for the creation of E_{11}^{*-} PL emission properties. In particular, molecular interactions of the substituents on the tube walls were found to be role of reaction modulators in the defect formation process. Accordingly, the defect binding configuration could be altered from a typical OrthoL90 to OrthoL30 relating to E_{11}^{*-} PL.

Furthermore, a click reaction at the doped sites in lf-SWCNTs-*o*A functionalized additional molecules via the CuAAC reaction pathway. Click chemistry, including CuAAC, is a powerful tool in organic chemistry and biochemistry, and abundant molecules and biomolecules can be easily conjugated.[50, 51] Therefore our alkyne-based molecular design in the *ortho*-substituted aryldiazonium salts allows for the functionalization of lf-SWCNTs by click chemistry-based post modification.

These findings contribute greatly to the development of various optical applications using NIR light >1000 nm; deep-tissue and high-resolution imaging/diagnosis probes for bio/medical applications based on second and third biological windows (1000–1350 nm for NIR-II and 1550–1870 nm for NIR-III), and single photon emitters at room temperature for quantum technologies such as quantum computing and quantum cryptographic communication, based on their telecom band wavelengths (>1250 nm). Therefore, the molecular chemistry approach opens new fields of molecularly designable lf-SWCNT creation for their widely modulated emission wavelengths.

Acknowledgements

This work was supported by Grant-in-Aids for JSPS KAKENHI Grant Number JP22H01910 and JP19H02557, the Research Grant from Kyushu University, and the Nanotechnology Platform Project, from the Ministry of Education, Culture, Sports, Science, and Technology, Japan.

Author contributions

T.S. and T.F. conceived and designed the project; B.Y., S.N., and H.A. performed the experiments; B.Y. and T.S. analyzed the data; B.Y. and K.K. performed the simulations; B.Y., T.F., and T.S. co-wrote the paper.

Data availability

The data supporting the findings of this study are available from the corresponding author, T.S., upon reasonable request.

Competing Interests

The authors declare no competing financial interests.

Reference

1. Tasis D., Tagmatarchis N., Georgakilas V., Prato M. Soluble Carbon Nanotubes. *Chem. Eur. J.* **9**, 4000-4008 (2003).

2. Fujigaya T., Nakashima N. Non-covalent polymer wrapping of carbon nanotubes and the role of wrapped polymers as functional dispersants. *Sci. Technol. Adv. Mater.* **16**, 024802 (2015).

3. Zaumseil J. Luminescent Defects in Single-Walled Carbon Nanotubes for Applications. *Adv. Optical. Mater.* **10**, 2101576 (2022).

4. Shiraki T. Molecular Functionalization of Carbon Nanotubes towards Near Infrared Photoluminescent Nanomaterials. *Chem. Lett.* **50**, 397-404 (2021).

5. Shiraki T., Miyauchi Y., Matsuda K., Nakashima N. Carbon Nanotube Photoluminescence Modulation by Local Chemical and Supramolecular Chemical Functionalization. *Acc. Chem. Res.* **53**, 1846-1859 (2020).

6. Gifford B.J., Kilina S., Htoon H., Doorn S.K., Tretiak S. Controlling Defect-State Photophysics in Covalently Functionalized Single-Walled Carbon Nanotubes. *Acc. Chem. Res.* **53**, 1791-1801 (2020).

7. Brozena A.H., Kim M., Powell L.R., Wang Y. Controlling the optical properties of carbon nanotubes with organic colour-centre quantum defects. *Nat. Rev. Chem.* **3**, 375-392 (2019).

8. Jorio A., Dresselhaus G., Dresselhaus M.S. *Carbon Nanotubes: Advanced Topics in the Synthesis, Structure, Properties and Applications*, Vol. 111 (2008).

9. Weisman R.B., Kono J. *Handbook of Carbon Nanomaterials*. World Scientific (2019).

10. Bachilo S.M., *et al.* Structure-Assigned Optical Spectra of Single-Walled Carbon Nanotubes. *Science* **298**, 2361-2366 (2002).

11. Crochet J., Clemens M., Hertel T. Quantum yield heterogeneities of aqueous single-wall carbon nanotube suspensions. *J. Am. Chem. Soc.* **129**, 8058-8059 (2007).

12. Scholes G.D., *et al.* Low-Lying Exciton States Determine the Photophysics of Semiconducting Single Wall Carbon Nanotubes. *J. Phys. Chem. C* **111**, 11139-11149 (2007).

13. Piao Y., *et al.* Brightening of carbon nanotube photoluminescence through the incorporation of sp 3 defects. *Nat. Chem.* **5**, 840-845 (2013).

14. Kwon H., *et al.* Molecularly Tunable Fluorescent Quantum Defects. *J. Am. Chem. Soc.* **138**, 6878-6885 (2016).

15. Shiraki T., Onitsuka H., Shiraishi T., Nakashima N. Near infrared photoluminescence modulation of single-walled carbon nanotubes based on a molecular recognition approach. *Chem. Commun.* **52**, 12972-12975 (2016).

16. Onitsuka H., Fujigaya T., Nakashima N., Shiraki T. Control of the Near Infrared Photoluminescence of Locally Functionalized Single‐Walled Carbon Nanotubes via Doping by Azacrown‐Ether Modification. *Chem. Eur. J.* **24**, 9393-9398 (2018).

17. Shiraki T., *et al.* Multistep Wavelength Switching of Near‐Infrared Photoluminescence Driven by Chemical Reactions at Local Doped Sites of Single‐Walled Carbon Nanotubes. *Chem. Eur. J.* **24**, 19162-19165 (2018).

18. Shiraki T., Shiraishi T., Juhász G., Nakashima N. Emergence of new red-shifted carbon nanotube photoluminescence based on proximal doped-site design. *Sci. Rep.* **6**, 28393 (2016).

19. Shiraki T., Yu B., Shiraishi T., Shiga T., Fujigaya T. Meta-linkage Design of Bis-aryldiazonium Modifiers for Wavelength Tuning of Near Infrared Photoluminescence from Locally Functionalized Single-walled Carbon Nanotubes. *Chem. Lett.* **48**, 791-794 (2019).

20. Fagan J.A., *et al.* Isolation of Specific Small-Diameter Single-Wall Carbon Nanotube Species via Aqueous Two-Phase Extraction. *Adv. Mater.* **26**, 2800-2804 (2014).

21. Podlesny B., Shiraki T., Janas D. One-step sorting of single-walled carbon nanotubes using aqueous two-phase extraction in the presence of basic salts. *Sci. Rep.* **10**, 9250 (2020).

22. He X., *et al.* Tunable room-temperature single-photon emission at telecom wavelengths from sp3 defects in carbon nanotubes. *Nat. Photon.* **11**, 577 (2017).

23. Berger F.J., *et al.* Brightening of Long, Polymer-Wrapped Carbon Nanotubes by sp3 Functionalization in Organic Solvents. *ACS Nano* **13**, 9259-9269 (2019).

24. Niidome Y., Yu B., Juhasz G., Fujigaya T., Shiraki T. Structure Dependence of Photoluminescence Solvatochromic Energy Shifts Based on Exciton Localization in Locally Functionalized Single-Walled Carbon Nanotubes. *J. Phys. Chem. C* **125**, 12758-12766 (2021).

25. Maeda Y., *et al.* Tuning of the photoluminescence and up-conversion photoluminescence properties of single-walled carbon nanotubes by chemical functionalization. *Nanoscale* **8**, 16916-16921 (2016).

26. Maeda Y., *et al.* Influence of local strain caused by cycloaddition on the band gap control of functionalized single-walled carbon nanotubes. *RSC advances* **9**, 13998-14003 (2019).

27. Dyke C.A., Stewart M.P., Maya F., Tour J.M. Diazonium-Based Functionalization of Carbon Nanotubes: XPS and GC-MS Analysis and Mechanistic Implications. *Synlett* **2004**, 155-160 (2004).

28. Schmidt G., Gallon S., Esnouf S., Bourgoin J.-P., Chenevier P. Mechanism of the Coupling of Diazonium to Single-Walled Carbon Nanotubes and Its Consequences. *Chem. Eur. J.* **15**, 2101-2110 (2009).

29. Gifford B.J., *et al.* Optical Effects of Divalent Functionalization of Carbon Nanotubes. *Chem. Mater.* **31**, 6950-6961 (2019).

30. Gifford B.J., Kilina S., Htoon H., Doorn S.K., Tretiak S. Exciton localization and optical emission in aryl-functionalized carbon nanotubes. *J. Phys. Chem. C* **122**, 1828-1838 (2018).

31. Saha A.*, et al.* Narrow-band single-photon emission through selective aryl functionalization of zigzag carbon nanotubes. *Nat. Chem.* **10**, 1089-1095 (2018).

32. Gifford B.J.*, et al.* Mod (nm, 3) Dependence of Defect-State Emission Bands in Aryl-Functionalized Carbon Nanotubes. *Nano Lett.* **19**, 8503-8509 (2019).

33. Shiraki T., Uchimura S., Shiraishi T., Onitsuka H., Nakashima N. Near infrared photoluminescence modulation by defect site design using aryl isomers in locally functionalized single-walled carbon nanotubes. *Chem. Commun.* **53**, 12544-12547 (2017).

34. Weisman R.B., Bachilo S.M. Dependence of Optical Transition Energies on Structure for Single-Walled Carbon Nanotubes in Aqueous Suspension: An Empirical Kataura Plot. *Nano Lett.* **3**, 1235-1238 (2003).

35. Dresselhaus M.S., Dresselhaus G., Saito R., Jorio A. Raman spectroscopy of carbon nanotubes. *Phys. Rep.* **409**, 47-99 (2005).

36. Maki H., Sato T., Ishibashi K. Direct Observation of the Deformation and the Band Gap Change from an Individual Single-Walled Carbon Nanotube under Uniaxial Strain. *Nano Lett.* **7**, 890-895 (2007).

37. Li Z.*, et al.* Efficient strain modulation of 2D materials via polymer encapsulation. *Nat. Commun.* **11**, 1151 (2020).

38. He X.*, et al.* Low-Temperature Single Carbon Nanotube Spectroscopy of sp(3) Quantum Defects. *ACS Nano* **11**, 10785-10796 (2017).

39. Blanch A.J., Lenehan C.E., Quinton J.S. Dispersant Effects in the Selective Reaction of Aryl Diazonium Salts with Single-Walled Carbon Nanotubes in Aqueous Solution. *J. Phys. Chem. C* **116**, 1709-1723 (2012).

40. Luo Z., Papadimitrakopoulos F., Doorn S.K. Electron-phonon interaction and its influence on reconstruction of single-walled carbon nanotube radial breathing mode spectra. *Appl. Phys. Lett.* **88**, 073110 (2006).

41. Saito R., Fujita M., Dresselhaus G., Dresselhaus M.S. Electronic structure of chiral graphene tubules. *Appl. Phys. Lett.* **60**, 2204-2206 (1992).

42. Luo Z., Pfefferle L.D., Haller G.L., Papadimitrakopoulos F. (n,m) Abundance Evaluation of Single-Walled Carbon Nanotubes by Fluorescence and Absorption Spectroscopy. *J. Am. Chem. Soc.* **128**, 15511-15516 (2006).

43. Settele S.*, et al.* Synthetic control over the binding configuration of luminescent sp 3-defects in single-walled carbon nanotubes. *Nature communications* **12**, 1-10 (2021).

44. Kolb H.C., Finn M.G., Sharpless K.B. Click Chemistry: Diverse Chemical Function from a Few Good Reactions. *Angew. Chem. Int. Ed.* **40**, 2004-2021 (2001).

45. Mann F.A., Herrmann N., Opazo F., Kruss S. Quantum Defects as a Toolbox for the Covalent Functionalization of Carbon Nanotubes with Peptides and Proteins. *Angew. Chem. Int. Ed.* **59**, 17732-17738 (2020).

46. Babiuch K.*, et al.* Functionalized, Biocompatible Coating for Superparamagnetic Nanoparticles by Controlled Polymerization of a Thioglycosidic Monomer. *Biomacromolecules* **12**, 681-691 (2011).

47. Loudy C.M.*, et al.* Revealing surface functionalities via microwave for the para-fluoro-Thiol click reaction. *Polymer* **202**, 122675 (2020).

48. Tuci G.*, et al.* Surface engineering of chemically exfoliated MoS2 in a “click”: How to generate versatile multifunctional transition metal dichalcogenides-based platforms. *Chem. Mater.* **30**, 8257-8269 (2018).

49. Sun L., Qian X., Ding C., An X. Integration of graft copolymerization and ring-opening reaction: a mild and effective preparation strategy for “clickable” cellulose fibers. *Carbohydr. Polym.* **198**, 41-50 (2018).

50. Parker C.G., Pratt M.R. Click Chemistry in Proteomic Investigations. *Cell* **180**, 605-632 (2020).

51. Neumann S., Biewend M., Rana S., Binder W.H. The CuAAC: Principles, Homogeneous and Heterogeneous Catalysts, and Novel Developments and Applications. *Macromol. Rapid Commun.* **41**, 1900359 (2020).